THE JOURNAL OF PHYSICAL CHEMISTRY B

Article

pubs.acs.org/JPCB

Lipid Bilayer Membrane Affinity Rationalizes Inhibition of Lipid Peroxidation by a Natural Lignan Antioxidant

Pavlína Podloucká,[†] Karel Berka,[†] Gabin Fabre,[†,‡] Markéta Paloncýová,[†] Jean-Luc Duroux,[‡] Michal Otyepka,*[,†] and Patrick Trouillas*[,†,‡,§]

[†]Regional Centre of Advanced Technologies and Materials, Department of Physical Chemistry, Faculty of Science, Palacký University, tř. 17 listopadu 12, 771 46 Olomouc, Czech Republic

[‡]INSERM UMR-S850 / LCSN EA1069, Faculté de Pharmacie, Université de Limoges, 2 rue de Dr. Marcland, 87025 Limoges, France

[§]Service de Chimie des Matériaux Nouveaux, Université de Mons-UMONS, Place du Parc 20, 7000 Mons, Belgium

Supporting Information

ABSTRACT: Lipid peroxidation is a degenerative oxidative process that modifies the structure of membranes, influencing their biological functions. Lignans, natural polyphenolic antioxidants widely distributed in plants, can prevent this membrane damage by free-radical scavenging. Here, we rationalize the difference in lipid peroxidation inhibition activity of argenteane, a natural dilignan isolated from wild nutmeg, and 3,3′-dimethoxy-1,1′-biphenyl-2,2′-diol, which represents the central part of argenteane responsible for its antioxidant activity. Although both compounds have the same capacity to scavenge free radicals, argenteane is a more active inhibitor of lipid peroxidation. We show that both compounds penetrate into DOPC and PLPC lipid bilayers and adopt similar positions and orientations, which therefore does not explain the difference in their lipid peroxidation inhibition activity. However, free energy profiles indicate that argenteane has a significantly higher affinity to the lipid bilayer, and thus a higher effective concentration to scavenge radicals formed during lipid peroxidation. This finding explains the higher activity of argenteane to inhibit lipid peroxidation.

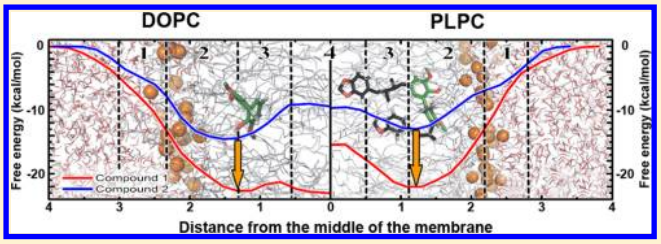

INTRODUCTION

Lipid peroxidation is a three-stage (initiation/propagation/termination) oxidative process occurring in lipid bilayer membranes. It is initiated by reactive species, mainly reactive oxygen species (ROS), induced endogenously by classical biochemical reactions or exogenously by, e.g., pollution or UV light. Lipid peroxidation may strongly modify the lipid bilayer structure, subsequently disrupting various key cell functions associated with membranes. Lipid peroxidation contributes to several pathologies, including neurodegenerative diseases, heart disease, atherosclerosis, liver disease, and aging processes.[1−6] The oxidative-induced degradation of membranes originates from the formation of aldehydes or lipid peroxides, acyl chain fragments, lipid−lipid cross-linked products, intramolecular cycles, etc.[7] Lipid bilayers composed of unsaturated fatty acids are more sensitive to such oxidative damage.

Natural antioxidants can prevent membrane damage, mainly by free-radical scavenging at either the initiation or the propagation stages.[8] Lignans are polyphenols widely distributed in plants. Being present in cereals, fruit, spices, beans, and other vegetables, they are natural components of the human diet.[9] Their chemical structure is derived from substituted cinnamic alcohols, and they are classified into six subgroups (dibenzylbutanes and skeletons with rings monofuranic lignans, butyrolactones, arylnaphthalenes, dibenzocyclolactones, furanofuranic lignans).[10,11] Lignans exhibit numerous biological activities, including antioxidant, antiproliferative, and protective functions against cardiovascular diseases and other degenerative pathologies associated with oxidative stress.[9,12−17] As for other polyphenols, their antioxidant activity is attributed to their capacity for H-atom transfer (HAT) from the OH groups to the free radicals.[18]

Argenteane (biserythro-5,5′-bis[1-(4-hydroxyl-3-methoxyphenyl)-4-(3,4-methylenedioxyphenyl)-2,3-dimethylbutane]) (**1**) is a natural dilignan isolated from wild nutmeg (Figure 1A).[19] Its antioxidant activity has been shown in vitro and compared to the activity of 3,3′-dimethoxy-1,1′-biphenyl-2,2′-diol (**2**), which mimics the central moiety of compound **1** (Figure 1).[18] Both compounds exhibited exactly the same capacity to scavenge DPPH (2,2-diphenyl-1-picrylhydrazyl radical), which was rationalized by quantum calculations showing exactly the same capacity for HAT.[20] However, compound **1** was 4 times more active than **2** at lipid peroxidation inhibition as measured on PLPC (1-palmitoyl-2-linoleoyl-*sn*-glycero-3-phosphatidylcholine) vesicles.[18] Moreover, compound **1** has an equivalent activity to vitamin E,

Received: December 27, 2012
Revised: April 4, 2013
Published: April 5, 2013

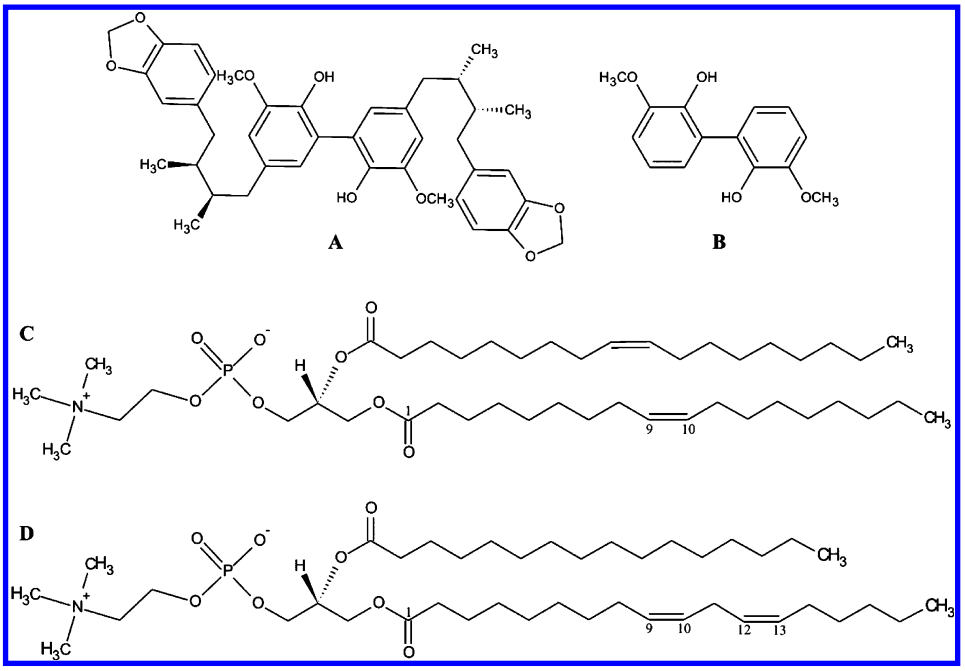

Figure 1. Chemical structures of (A) argenteane (compound **1**), (B) 3,3′-dimethoxy-1,1′-biphenyl-2,2′-diol (compound **2**), (C) 1,2-dioleoyl-*sn*-glycero-3-phosphatidylcholine (DOPC), and (D) 1-palmitoyl-2-linoleoyl-*sn*-glycero-3-phosphatidylcholine (PLPC).

Table 1. Average Distances (nm) Given with Respect to the Center of the Lipid Bilayers, with the Corresponding Standard Deviations Calculated for the OH Groups in Both the DOPC and PLPC Lipid Bilayers[a]

	position of COM (nm)		position OH groups (nm)		overlap of OH groups and double bond (%)		$\Delta G(z_{min})$ (kcal/mol)		IC_{50} (μM)	
compd	DOPC	PLPC	DOPC	PLPC	DOPC	PLPC	DOPC	PLPC	DPPH scavenging[b]	lipid peroxidation inhibition[b]
1	1.4 ± 0.2	1.2 ± 0.2	1.5 ± 0.2	1.3 ± 0.2	29 ± 15	23 ± 4	−22.7 ± 0.2	−21.9 ± 0.6	70 ± 2	0.68 ± 0.04
2	1.6 ± 0.2	1.3 ± 0.2	1.7 ± 0.2	1.3 ± 0.3	13 ± 6	19 ± 2	−14.5 ± 0.1	−12.8 ± 1.1	70 ± 4	2.70 ± 0.05

[a]All distances were averaged over the last 150 ns of unbiased MD simulations. $\Delta G(z_{min})$ reflects the affinity of compound to membrane. DPPH scavenging and lipid peroxidation inhibition activities of compounds **1** and **2** were taken from the literature.[18] [b]Data from ref 18.

which is well-known as a powerful lipid peroxidation inhibitor (Table 1). Due to the presence of nonpolar side chains in compound **1**, the capacity to incorporate into lipid bilayers was proposed to explain such a difference in activity.

In this study, we aimed to rationalize the different capacities of both compounds (**1** and **2**) to inhibit lipid peroxidation on PLPC membranes.[18] The pair of compounds **1** and **2** provides a useful basis to establish a fine structure activity relationship at the atomic level because both compounds share the same central moiety but differ in the presence/absence of long nonpolar side chains. We calculated the average positions and orientations of both compounds either on the PLPC or DOPC bilayers by molecular dynamics (MD) simulations. MD simulations have been repeatedly shown to provide useful information on the interaction of small molecules with lipid membranes[21−31] providing a unique view at both an atomic scale and subpicosecond time resolution. The affinity of both compounds to lipid bilayers was investigated in terms of free energy profiles calculated along the bilayer normal. The results showed that both compounds adopt similar positions in the lipid bilayers, but they have significantly different affinities to lipid bilayers as compound **1** exhibited a significantly higher free energy difference between water and lipid phases than compound **2**. This finding may explain the higher activity of compound **1** to inhibit lipid peroxidation.

METHODOLOGY

Two types of lipids, namely DOPC (1,2-dioleoyl-*sn*-glycero-3-phosphatidylcholine) as the most abundant lipid in mammal cell membranes[32] and PLPC (1-palmitoyl-2-linoleoyl-*sn*-glycero-3-phosphatidylcholine), were used as membrane models to explain experimentally observed differences in the lipid peroxidation activity of compounds **1** and **2**.[18] Pure phospholipid bilayers are generally accepted to exhibit many of the important features of real membranes.[33] The former model comprised 128 DOPC molecules, in which the oleoyl chains contain one double bond between carbons C_9 and C_{10} (Figure 1C). The latter model contained 144 PLPC molecules. For these phospholipids, the palmitic chain is a fully saturated fatty acid, whereas the linoleyl chain contains two double bonds (C_9═C_{10} and C_{12}═C_{13}, Figure 1D). The presence of the double bonds makes PLPC more sensitive to oxidation. In both lipid bilayer models, both leaflets contain the same number of molecules. The structures of the lipids were taken from the literature[34,35] and a united-atom Berger's force field was used.[36] The bilayers were oriented perpendicularly to the *z*-axis of the box containing the molecular assembly. The bilayers were first equilibrated in the absence of any solute (**1** and **2**). They were surrounded by an explicit SPC water model[37] and the physiological concentration of NaCl (0.15 mol·L^{-1}) in water was used. The MD simulations were carried out using the

dx.doi.org/10.1021/jp3127829 | J. Phys. Chem. B 2013, 117, 5043−5049

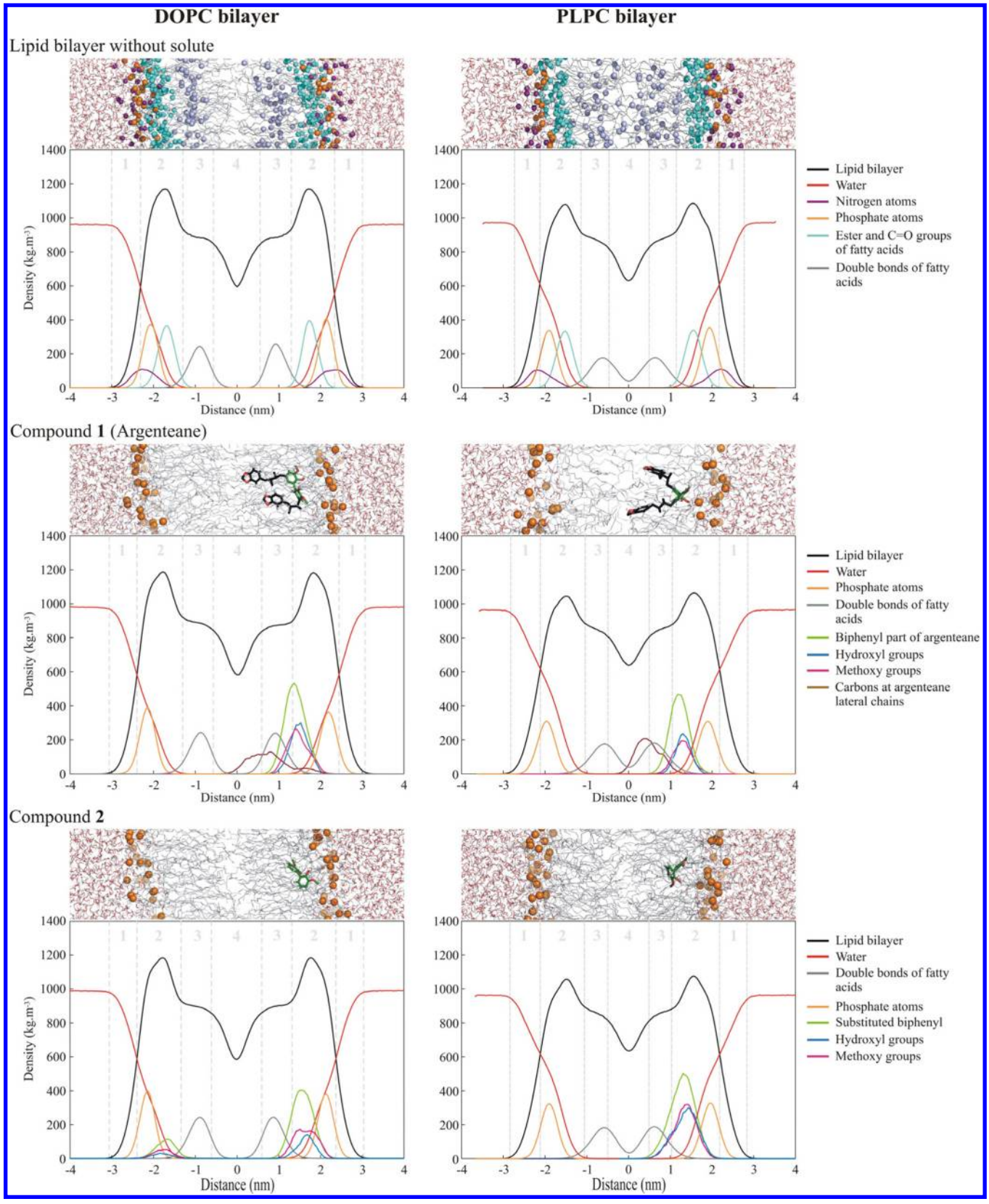

Figure 2. Characteristic snapshots and mass density profiles of DOPC and PLPC bilayers in the absence (upper panel) or presence (middle and lower panel) of **1** and **2**. For clarity, the components (and corresponding densities) are shown in different colors according to the legend and the density profiles of the studied compounds are scaled. The boundaries of regions 1−4 are shown in the upper part of the graphs.

GROMACS 4.0.7 package[38] with periodic boundary conditions in all directions.

The conformations of **1** and **2** were optimized using the hybrid DFT functional B3P86 combined with the 6-31+G(d,p)

dx.doi.org/10.1021/jp3127829 | J. Phys. Chem. B 2013, 117, 5043−5049

basis set B3P86/6-31+G(d,p), which has been well adapted for the description of polyphenols.[39] The topology was generated from the PRODRG2 Beta server using the Gromos53a6 force field.[40] The partial atomic charges were assigned using the program Antechamber[41] and RESP method[42] after single-point calculation at the HF/6-31G* level. Optimization and single-point calculations were carried out in Gaussian03.[43]

For both lipid bilayers, several MD simulations were carried out from different initial orientations and positions (in the middle of the lipid bilayer or outside the bilayer in the bulk water). To avoid unfavorable atomic contacts, the initial structures were first minimized by the steepest descent method and then equilibrated during a 200 ps simulation. During the equilibration step, the system was heated to 310 K by employing a v-rescale thermostat.[44] The pressure was kept constant using the anisotropic Berendsen barostat[45] at 1 bar. All bonds were constrained by the LINCS algorithm.[46] The electrostatic interactions were evaluated using the smooth particle-mesh Ewald method[47,48] with a maximum spacing for the FFT grid of 0.12 nm. Both the Coulomb and Lennard-Jones interactions were truncated at 1.4 nm.

The equilibration step was followed by a 300 ns simulation. Thirteen independent unbiased simulations were carried out, differing in starting positions of the compounds. For each simulation the following protocol was used. The temperature was kept constant at 310 K by the v-rescale thermostat[44] with 0.1 ps coupling. The anisotropic Parrinello−Rahman barostat[49] was used to keep the pressure at 1 bar with a coupling time constant of 1.0 ps and compressibility of 4.5×10^{-5} bar^{-1}. Integration of Newton's equations was based on the leapfrog algorithm using 2 fs time steps.[50] The electrostatic interactions were computed by the smooth particle-mesh Ewald method[47,48] with a space cutoff at 1.4 nm and fast-Fourier grid space of 0.12 nm. The same cutoff was used for short-range interactions. The MD simulations were performed with different random initial velocities sampled according to a Maxwell distribution. All bonds were constrained using the LINCS algorithm.[46] The trajectories were visualized with VMD.[51]

Partitioning into the membrane was computed using the potential of mean force method to obtain free energy profiles[23,52−54] A series of initial structures was obtained from unbiased MD simulations to define windows along the bilayer normal (z-axis) separated by 0.10 ± 0.02 nm. In the case of missing windows, 15 ns pulling simulations were performed. In the latter simulations, the molecule was pulled from the center of the lipid bilayer (z = 0 nm) to the edge of the box along the z-axis. The rate of change of the reference position was 0.0005 nm/ps. In all windows, the center of mass (COM) of the biphenyl moiety was constrained in that specific depth and the force applied to the molecule was monitored. Neale et al. showed that relatively long simulation times are required for each window to achieve convergence in umbrella simulations with charged solutes,[55] and Singh and Tieleman[56] highlighted a necessity of simulation time longer than the slowest relaxation in a system. We recently showed[22] that constraint simulations may converge more quickly (the estimated free energies became constant in time) and also that 0.2 nm separation of simulation frames in constraint simulation is sufficient for construction of free energy profiles. In the present work, 50 and 80 ns windows of constraint simulation were used in DOPC and PLPC, respectively. The free energy profiles were reconstructed from the last 30 ns. They were calculated as a function of the distance of the antioxidant biphenyl moiety from the bilayer center according to the eq 1[23,29]

$$\Delta G(z) = -\int_{z=\infty}^{z} \langle F(z') \rangle_t \, dz' \quad (1)$$

where $\langle F(z') \rangle_t$ is the average force constraining the biphenyl moiety at a specific position of the simulation. Due to the symmetry of the lipid bilayer, the profile of ΔG was calculated for only half of the box. The error estimates were calculated as a standard deviation of the mean of the constraining force integrated over the z-axis. We assume that error bars may be underestimated.[22] For comparison, the free energy profile of compound **2** interacting with PLPC was calculated using 30 ns per simulation window (Figure S4 in the Supporting Information).

The overlap of OH groups of both compounds with lipid double bonds was calculated as an integral over product of normalized densities of both groups along the bilayer normal (Figure S1 and Table S1 in the Supporting Information) according to eq 2

$$S = \int_{-\infty}^{\infty} a(x)b(x) \, dx \quad (2)$$

where $a(x)$ and $b(x)$ are normalized functions of density profiles of OH groups and double bonds. Last 150 ns of unbiased simulations were used for the calculation.

RESULTS AND DISCUSSION

Comparison of the PLPC and DOPC Lipid Bilayers in the Absence of Solute. Both DOPC and PLPC bilayers exhibited typical features of unsaturated lipid bilayers. Four regions could clearly be distinguished according to the Marrink and Berendsen membrane model,[23] namely the low headgroup density in direct contact with the water phase (region 1), the high headgroup density defining an intermediate region between the water and lipid phases (region 2), the lipid chains (region 3), and the center of the membrane (region 4) with low lipid density (Figure 2). The flexible arrangement of the lipid chains shows that both bilayers were in their liquid phases at 310 K (Figure 2). The area per lipid was 0.59 and 0.63 nm^2 for the DOPC and PLPC bilayers, respectively, during the simulation. Therefore, in DOPC, the two similar chains containing one double bond allow better lateral packing. In PLPC, the two double bonds in one of the lipid chains produce a kink in the fatty acid chains, disfavoring tight interchain packing (Figure 1), making the bilayer more fluid.[33] However, in the PLPC bilayer, the presence of a shorter saturated chain and the polyunsaturated chain favor better packing along the z-axis and thus a lower thickness, which was by 0.8 nm smaller than that of the DOPC bilayer.

Simple Penetration Process of Compounds 1 and 2. When starting outside of the bilayer, both compounds **1** and **2** intercalated spontaneously between lipid chains (Figure S2 in the Supporting Information), regardless of the type of lipid bilayer used for the unbiased simulations. When starting inside, both compounds stayed in the bilayers. This is attributed to their amphiphatic character. However, a thorough analysis of the unbiased MD simulations showed that the compounds behaved in different ways regarding the penetration process.

When starting out of the bilayer, compound **1** first approached the polar surface, then slowly passed through the polar region, and finally reached its equilibrated position close to the headgroup area of the lipid bilayer (between regions 2

dx.doi.org/10.1021/jp3127829 | J. Phys. Chem. B 2013, 117, 5043−5049

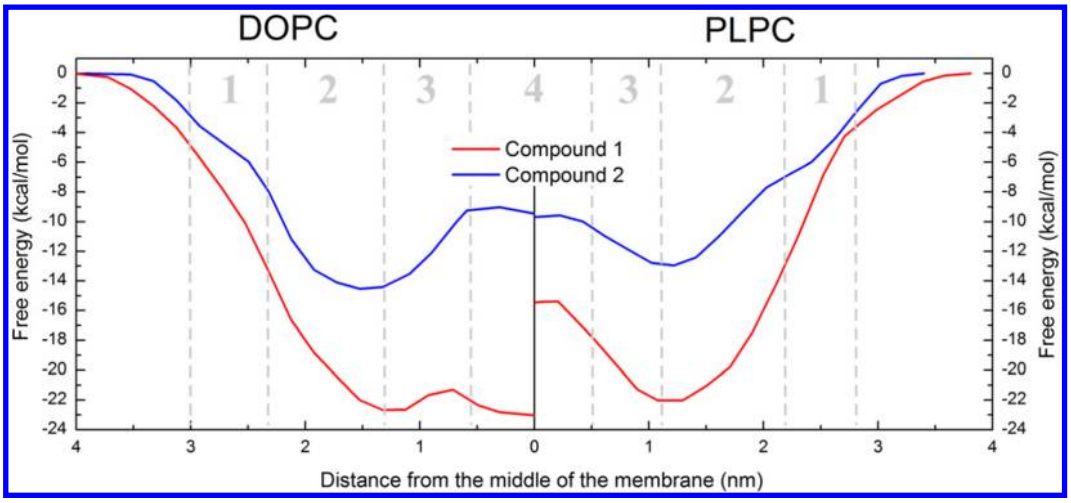

Figure 3. Free energy profiles of compounds **1** and **2** along the *z*-axis in the DOPC (left) and PLPC (right) lipid bilayers shown for one leaflet.

and 3). The whole process took approximately 200 and 50 ns in the DOPC and PLPC bilayers, respectively. When starting in the center of the bilayer, compound **1** reached its equilibrated position during the first 50 ns in both lipid bilayers. This highlights that the most time-consuming process is transport through regions 1 and 2, in which the water molecules and the polar groups of the membrane create a complex network of hydrogen bonds. Due to its size, the presence of OH groups and two benzodioxole moieties, compound **1** made many intermolecular interactions in these regions, which slowed down the diffusion movement to its equilibrium position. Compound **2** also accumulated inside both bilayers close to the polar groups of the lipids (in region 2). However, due to the absence of the benzodioxole moieties and its smaller size compared to **1**, the equilibrated position of **2** was reached within 50 ns regardless of the starting point, i.e., inside or outside the bilayer.

Location and Orientation of Compounds 1 and 2, and Their Antioxidant-Active OH Groups in Lipid Bilayers. The COM of the central guaiacyl moiety of **1** (responsible for the free radical scavenging capacity of **1**)[18] was located at 1.4 ± 0.2 and 1.2 ± 0.2 nm from the center of the DOPC and PLPC bilayers, respectively (Figure 2 and Table 1). This confirms that the molecule was equilibrated in region 2, close to the boundary between regions 2 and 3. The two lateral benzodioxole moieties of **1** were very flexible in all free MD simulations. The mass densities of these lateral moieties were widely distributed from region 2 up to region 4. Having no role in free-radical scavenging, the benzodioxole moieties may participate in the antioxidant action (lipid peroxidation inhibition) from a conformational aspect. The global effect of their presence is a subtle balance between their role as anchor (favoring insertion deep in the membrane) and their steric interaction (disfavoring membrane penetration).

The OH groups of the guaiacyl moiety are the H-atom donors, responsible for the free-radical scavenging activity of **1**.[18] They were oriented toward the bilayer surface. Such an orientation was driven by hydrogen-bonding interactions between these groups and both the polar head groups of the bilayer and the water molecules, which penetrated into region 2. It should be noted that the oxygen atoms of the benzodioxole moiety (Figure 1) interacted with neither the polar head groups nor the penetrating water molecules.

In order to establish a correlation between the location of the free-radical-scavenger-active groups and the region in which the propagation stage of lipid peroxidation occurs, an overlapping between both OH groups of the antioxidant and double bonds of unsaturated fatty acids was averaged over the MD simulations (Table S1, Figures S1 and S2 in the Supporting Information). For compound **1**, the OH groups are the only free-radical scavengers; thus, the greater the overlap, the more efficient ROO$^{\bullet}$ free radical scavenging by the antioxidant. In contrast, it is noteworthy that the lower the overlap, the less efficient its role in the propagation stage, and the more probable its role in the initiation stage (i.e., scavenging of the free radicals penetrating the membrane to oxidize lipids). This overlap was 29 ± 15 and 23 ± 4% for compound **1** in the DOPC and PLPC lipid bilayer, respectively.

For compound **2**, the distance of the COM was 1.6 ± 0.2 and 1.3 ± 0.2 nm from the center of the DOPC and PLPC lipid bilayers, respectively, suggesting it is embedded in region 2 also close to the boundary between regions 2 and 3. In the case of the DOPC bilayer, the density of **2** exhibited two maxima in both leaflets (Figure 2, and Figure S1 in the Supporting Information), indicating that this compound (even during free MD simulations) passed through the lipid bilayer (Figure S2 in the Supporting Information), whereas this behavior was not observed with compound **1**, possibly as **1** is larger and therefore its diffusion through the center of bilayer will be slower.

As for compound **1**, the OH groups of both guaiacyl moieties of compound **2** were also oriented toward the polar head groups of the bilayers, creating hydrogen bonds with the phosphates and water molecules inserted in region 2. Broad density profiles were obtained (Figure 2), indicating that the molecule fluctuated significantly during the simulations (Figure S2). The overlap of the OH groups of **2** with the double bonds of the unsaturated fatty acids was lower than for **1**, mainly in the DOPC membrane (13 ± 6% and 19 ± 2% in the DOPC and PLPC bilayers, respectively). The lower overlap observed in DOPC compared to PLPC originated from the closer location of compound **2** to the center of the PLPC lipid bilayer. In addition, the mobility of **2** was slightly higher in PLPC (see the standard deviation for the OH group in Table 1), probably due to the higher fluidity of this lipid bilayer. However, the lipid peroxidation inhibition activity was measured on PLPC vesicles, whereas only marginal differences were found for the PLPC bilayer, either in overlap of OH groups and lipid double bonds

dx.doi.org/10.1021/jp3127829 | J. Phys. Chem. B 2013, 117, 5043−5049

or in location and orientation. These differences cannot therefore explain the dramatic decrease in lipid peroxidation inhibition from **1** to **2**.

Free Energy Profiles for the Membrane Penetration of 1 and 2. The free energy profile of compound **1** exhibited a relatively broad minimum at 1.3 nm for both bilayers. The free energy minimum was located at -22.7 ± 0.2 and -21.9 ± 0.6 kcal/mol with respect to the water phase in the DOPC and PLPC bilayers (Figure 3), respectively. The free energy profile performed in the DOPC bilayer exhibited a second minimum in the middle of the membrane. This position is surprisingly as stable as the former one (Figure 3), which reflects that the DOPC bilayer has an interstitial space in between both leaflets, large enough for compound **1** to adapt and stabilize. Moreover, the energetic barrier for the flip-flop of this compound from one to the other leaflet was low in the DOPC bilayer (1.5 ± 0.1), while it was significantly higher in the PLPC bilayer (6.6 ± 0.4 kcal/mol).

Compound **2** was predicted to have a lower affinity to both membranes than compound **1**. The free energy minima ($\Delta G(z_{min})$) were at 1.5 and 1.2 nm in the DOPC and PLPC bilayers stabilized by -14.5 ± 0.1 and -12.8 ± 1.1 kcal/mol, respectively (Figure 3). The barrier of passage from one to the other leaflet was 5.5 ± 0.1 and 3.4 ± 0.3 kcal/mol in DOPC and PLPC, respectively.

The free energy profiles indicate that both compounds have significantly different affinities to the lipid bilayers. Compound **1** displays higher affinity to both DOPC and PLPC membranes, which in turn indicates that the effective concentrations of compound **1** in both membranes are higher than concentrations of compound **2**, which is due to the presence of nonpolar side chains of compound **1**. The higher affinity of compound **1** to lipid bilayers can explain higher activity in lipid peroxidation inhibition measured on PLPC vesicles. It may also indicate higher activity on other types of unsaturated lipid bilayer, as is indicated from its affinity to DOPC bilayer (Table 1)

CONCLUDING REMARKS AND CORRELATION TO EXPERIMENTAL DATA

The present theoretical investigation rationalizes the difference in lipid peroxidation inhibition observed between compounds **1** and **2**, despite these two compounds exhibiting the same free-radical scavenging and HAT capacities. Molecular dynamic simulations identified differences in the membrane positions and orientations between the two compounds. However, these differences appeared marginal and not sufficient to rationalize the difference in lipid peroxidation inhibition activities of both compounds. On the other hand, biased MD simulations showed that the compounds significantly differed in their affinities to the lipid bilayers. Compound **1** was stabilized over compound **2** by 8.2 and 9.1 kcal/mol in DOPC and PLPC, respectively. This free energy difference can be associated to the difference in partitioning of both compounds into the lipid bilayer. Therefore, the effective concentration of compound **1** in the studied lipid membranes should be significantly higher than for compound **2**, in agreement with the efficient lipid peroxidation inhibition capacity of compound **1**. This molecular picture for membrane penetration of this compound demonstrates the role of the hydrophobic benzodioxole side moieties, which stabilize the active part of compound **1** between the lipid head groups and unsaturated parts of the lipid chains. Such a position enables inhibition of lipid peroxidation (i) during the initiation stage (i.e., scavenging of incoming free radicals following their uptake into the membrane) or (ii) during the propagation stage (i.e., propagation of the lipid-based $ROO^{\bullet}$ free radicals between lipid chains)

ASSOCIATED CONTENT

Supporting Information

Calculated overlaps of mass densities of OH groups and double bonds during unbiased simulation (Table S1); the density profiles of OH groups of studied compounds during free simulations (Figure S1); the positions of OH groups during unbiased simulations (Figure S2); plot of the free energy profiles vs simulation time (Figure S3); two independent free energy profiles of compound **2** on the PLPC bilayer (Figure S4). This material is available free of charge via the Internet at http://pubs.acs.org.

AUTHOR INFORMATION

Corresponding Author

*E-mail: michal.otyepka@upol.cz (M.O.); patrick.trouillas@unilim.fr (P.T.).

Notes

The authors declare no competing financial interest.

ACKNOWLEDGMENTS

The authors gratefully acknowledge support from the Operational Program Research and Development for Innovations—European Regional Development Fund (project CZ.1.05/2.1.00/03.0058 of the Ministry of Education, Youth and Sports of the Czech Republic), the Operational Program Education for Competitiveness—European Social Fund (projects CZ.1.07/2.3.00/20.0017 and CZ.1.07/2.3.00/20.0058 of the Ministry of Education, Youth and Sports of the Czech Republic), and the Grant Agency of the Czech Republic (P208/12/G016). The authors also thank the "Conseil Régional du Limousin" for financial support and CALI (CAlcul en LImousin). The research based in Limoges was also supported by the COST action CM0804 "Chemical Biology with Natural Compounds".

ABBREVIATIONS

DPPH radical, 2,2-diphenyl-1-picrylhydrazyl radical; DOPC, 1,2-dioleoyl-*sn*-glycero-3-phosphatidylcholine; PLPC, 1-palmitoyl-2-linoleoyl-*sn*-glycero-3-phosphatidylcholine; MD, molecular dynamics; BDE, bond dissociation enthalpy; IC_{50}, half-maximal inhibitory concentration; COM, center of mass

REFERENCES

(1) Reed, T. T. *Free Radical Biol. Med.* **2011**, *51*, 1302−1319.
(2) Steinberg, D. *Med. Sci. Symp. Ser.* **1998**, *12*, 141−147.
(3) Rikans, L. E.; Hornbrook, K. R. *BBA, Mol. Basis Dis.* **1997**, *1362*, 116−127.
(4) Praticò, D. *Science's SAGE KE* **2002**, *50*, re5.
(5) Halliwell, B.; Gutteridge, J. M. C. *Free Radicals in Biology and Medicine*, 4th ed.; Oxford University Press: Oxford, UK, 2007.
(6) Negre-Salvayre, A.; Auge, N.; Ayala, V.; Basaga, H.; Boada, J.; Brenke, R.; Chapple, S.; Cohen, G.; Feher, J.; Grune, T.; et al. *Free Radical Res.* **2010**, *44*, 1125−1171.
(7) Niki, E. *Free Radical Biol. Med.* **2009**, *47*, 469−484.
(8) Gutteridge, J. M. C. *Clin. Chem.* **1995**, *41*, 1819−1828.
(9) Adlercreutz, H. *Crit. Rev. Clin. Lab. Sci.* **2007**, *44*, 483−525.
(10) Moss, G. P. *Pure Appl. Chem.* **2000**, *72*, 1493−1523.
(11) Ward, R. S. *Nat. Prod. Rep.* **1999**, *16*, 75−96.
(12) Filleur, F.; Le Bail, J. C.; Duroux, J. L.; Simon, A.; Chulia, A. J. *Planta Medica* **2001**, *67*, 700−704.

(13) Adlercreutz, H. *Environ. Health Persp.* **1995**, *103*, 103−112.
(14) McCann, M. J.; Gill, C. I. R.; McGlynn, H.; Rowland, I. R. *Nutr. Cancer* **2005**, *52*, 1−14.
(15) Westcott, N. D.; Muir, A. D. *Phytochem. Rev.* **2003**, *2*, 401−417.
(16) Wang, L. Q. *J. Chromatogr. B* **2002**, *777*, 289−309.
(17) Ghisalberti, E. L. *Phytomedicine* **1997**, *4*, 151−166.
(18) Calliste, C. A.; Kozlowski, D.; Duroux, J. L.; Champavier, Y.; Chulia, A. J.; Trouillas, P. *Food Chem.* **2010**, *118*, 489−496.
(19) Filleur, F.; Pouget, C.; Allais, D. P.; Kaouadji, M.; Chulia, A. J. *Nat. Prod. Lett.* **2002**, *16*, 1−7.
(20) Anouar, E.; Calliste, C. A.; Košinová, P.; Di Meo, F.; Duroux, J. L.; Champavier, Y.; Marakchi, K.; Trouillas, P. *J. Phys. Chem. A* **2009**, *113*, 13881−13891.
(21) Košinová, P.; Berka, K.; Wykes, M.; Otyepka, M.; Trouillas, P. *J. Phys. Chem. B* **2012**, *116*, 1309−1318.
(22) Paloncýová, M.; Berka, K.; Otyepka, M. *J. Chem. Theory Comput.* **2012**, *8*, 1200−1211.
(23) Marrink, S. J.; Berendsen, H. J. C. *J. Phys. Chem.* **1994**, *98*, 4155−4168.
(24) Bemporad, D.; Essex, J. W.; Luttmann, C. *J. Phys. Chem. B* **2004**, *108*, 4875−4884.
(25) dos Santos, D. J. V. A.; Eriksson, L. A. *Biophys. J.* **2006**, *91*, 2464−2474.
(26) Eriksson, E. S. E.; dos Santos, D. J. V. A.; Guedes, R. C.; Eriksson, L. A. *J. Chem. Theory Comput.* **2009**, *5*, 3139−3149.
(27) Ulander, J.; Haymet, A. D. J. *Biophys. J.* **2003**, *85*, 3475−3484.
(28) Qin, S. S.; Yu, Z. W.; Yu, Y. X. *J. Phys. Chem. B* **2009**, *113*, 16537−16546.
(29) Boggara, M. B.; Krishnamoorti, R. *Biophys. J.* **2010**, *98*, 586−595.
(30) Vazdar, M.; Jurkiewicz, P.; Hof, M.; Jungwirth, P.; Cwiklik, L. *J. Phys. Chem. B* **2012**, *116*, 6411−6415.
(31) Paloncýová, M.; Berka, K.; Otyepka, M. *J. Phys. Chem. B* **2013**, *117*, 2403−2410.
(32) van Meer, G.; Voelker, D. R.; Feigenson, G. W. *Nat. Rev. Mol. Cell Biol.* **2008**, *9*, 112−124.
(33) Bruce, A.; Alexander, J.; Julian, L.; Martin, R.; Keith, R.; Peter, W. *Molecular Biology of the Cell*, 5th ed.; Garland Science: New York, 2008.
(34) Siu, S. W. I.; Vácha, R.; Jungwirth, P.; Bockmann, R. A. *J. Chem. Phys.* **2008**, *128*.
(35) Bachar, M.; Brunelle, P.; Tieleman, D. P.; Rauk, A. *J. Phys. Chem. B* **2004**, *108*, 7170−7179.
(36) Berger, O.; Edholm, O.; Jahnig, F. *Biophys. J.* **1997**, *72*, 2002−2013.
(37) Berendsen, H. J. C.; Postma, J. P. M.; van Gunsteren, W. F.; Hermans, J. *Intermolecular Forces*; Reidel Publishing Co.: Dordrecht, The Netherlands, 1981.
(38) Hess, B.; Kutzner, C.; van der Spoel, D.; Lindahl, E. *J. Chem. Theory Comput.* **2008**, *4*, 435−447.
(39) Trouillas, P.; Marsal, P.; Siri, D.; Lazzaroni, R.; Duroux, J. L. *Food Chem.* **2006**, *97*, 679−688.
(40) Schuttelkopf, A. W.; van Aalten, D. M. F. *Acta Crystallogr. D* **2004**, *60*, 1355−1363.
(41) Case, D. A.; Darden, T. A.; Cheatham, I., T. E.; Simmerling, C. L.; Wang, J.; Duke, R. E.; Luo, R.; Walker, R. C.; Zhang, W.; Merz, K. M.; et al. *AMBER 11*; University of California: San Francisco, 2010.
(42) Bayly, C. I.; Cieplak, P.; Cornell, W. D.; Kollman, P. A. *J. Phys. Chem.* **1993**, *97*, 10269−10280.
(43) Frisch, M. J.; Trucks, G. W.; Schlegel, H. B.; Scuseria, G. E.; Robb, M. A.; Cheeseman, J. R.; Montgomery, J. A., Jr.; Vreven, T.; Kudin, K. N.; Burant, J. C.; et al. *Gaussian 03, revision E.01*; Gaussian, Inc.: Wallingford, CT, 2004.
(44) Bussi, G.; Donadio, D.; Parrinello, M. *J. Chem. Phys.* **2007**, *126*.
(45) Berendsen, H. J. C.; Postma, J. P. M.; Vangunsteren, W. F.; Dinola, A.; Haak, J. R. *J. Chem. Phys.* **1984**, *81*, 3684−3690.
(46) Hess, B.; Bekker, H.; Berendsen, H. J. C.; Fraaije, J. G. E. M. *J. Comput. Chem.* **1997**, *18*, 1463−1472.
(47) Darden, T.; York, D.; Pedersen, L. *J. Chem. Phys.* **1993**, *98*, 10089−10092.
(48) Essmann, U.; Perera, L.; Berkowitz, M. L.; Darden, T.; Lee, H.; Pedersen, L. G. *J. Chem. Phys.* **1995**, *103*, 8577−8593.
(49) Parrinello, M.; Rahman, A. *J. Appl. Phys.* **1981**, *52*, 7182−7190.
(50) Hockney, R. W.; Goel, S. P.; Eastwood, J. W. *J. Comput. Phys.* **1974**, *14*, 148−158.
(51) Humphrey, W.; Dalke, A.; Schulten, K. *J. Mol. Graph.* **1996**, *14*, 33−38.
(52) Jämbeck, J. P. M.; Lyubartsev, A. P. *Phys. Chem. Chem. Phys.* **2013**, *15*, 4677−4686.
(53) Ingram, T.; Storm, S.; Kloss, L.; Mehling, T.; Jakobtorweihen, S.; Smirnova, I. V *Langmuir* **2013**, *29*, 3527−3537.
(54) Karlsson, B. C. G.; Olsson, G. D.; Friedman, R.; Rosengren, A. M.; Henschel, H.; Nicholls, I. *J. Phys. Chem. B* **2013**, *117*, 2384−95.
(55) Neale, C.; Bennett, W. F. D.; Tieleman, D. P.; Pomès, R. *J. Chem. Theory Comput.* **2011**, *7*, 4175−4188.
(56) Singh, G.; Tieleman, D. P. *J. Chem. Theory Comput.* **2013**, *9*, 1657−1666.